

## Perovskite oxide superlattices: Magnetotransport and magnetic properties

G. Q. Gong

*Department of Physics, Brown University, Providence, Rhode Island, 02912*

A. Gupta

*IBM Thomas J. Watson Research Center, Yorktown Heights, New York 10598*

Gang Xiao

*Department of Physics, Brown University, Providence, Rhode Island 02912  
and IBM Thomas J. Watson Research Center, Yorktown Heights, New York 10598*

P. Lecoeur and T. R. McGuire

*IBM Thomas J. Watson Research Center, Yorktown Heights, New York 10598*

(Received 21 March 1996)

We have fabricated perovskite superlattices consisting of two ferromagnetic metallic oxides:  $\text{La}_{0.67}\text{Ca}_{0.33}\text{MnO}_3$  (LCMO) and  $\text{SrRuO}_3$  (SRO). We have investigated the magnetotransport and magnetic properties of a series of samples, in which the layer thickness of LCMO is fixed and that of SRO varied from 0 to 20 unit cells. The magnetoresistance ratio in a superlattice can be increased by a factor of 3 at low temperatures over the MR ratio in pure LCMO film. This substantial enhancement is most likely caused by the interface spin-dependent scattering. The superlattice structure also increases  $T_c$  of LCMO by introducing a biaxial tension, and induces two consecutive switchings of magnetic easy axis direction with increasing SRO thickness. [S0163-1829(96)50430-3]

Doped perovskite  $\text{La}_{1-x}\text{A}_x\text{MnO}_3$  ( $A = \text{Ca}, \text{Ba}, \text{and Sr}$ ) systems exhibit extremely large magnetoresistance (MR) and diverse types of magnetic orderings.<sup>1-10</sup> At about  $x = 1/3$  doping level, the manganate is a ferromagnet (FM) with a large MR occurring around the magnetic transition temperature  $T_c$ . The MR is strongly dependent on temperature, having a maximum MR of a few hundred percent near  $T_c$  (for  $A = \text{Ca}$ ), but reducing to a few percent approaching 0 K.<sup>7-10</sup> The magnetotransport behavior can be attributed to a strong coupling between the conduction electrons and the local magnetic moments through a mechanism called Zener double exchange.<sup>3</sup> At high temperatures, the magnetic structure becomes dynamical, which leads to a substantial increase in resistivity. An external field suppresses the thermal spin fluctuation and reduces the resistivity. In this study, we explore a different method, other than using temperature, to affect the underlying magnetic structure in  $\text{La}_{0.7}\text{Ca}_{0.3}\text{MnO}_3$  (LCMO). We have made a series of superlattices by combining LCMO with another FM perovskite oxide,  $\text{SrRuO}_3$  (SRO).<sup>11-14</sup> We have found that the superlattice structure has profound influences on the magnetic phase transition, anisotropy, and hysteresis of the manganate. The magnetotransport is also strongly affected by the layering. In particular, a large enhancement of the MR ratio is obtained at low temperatures in the superlattices. This is an indication of the emergence of a different magnetotransport mechanism not related to the dynamical magnetic structure, which we attribute to the spin-dependent scattering at the interfaces.

We have grown LCMO/SRO superlattices on (100)-oriented  $\text{SrTiO}_3$  substrates using a multitarget pulsed laser deposition system.<sup>15</sup> The two targets,  $\text{La}_{0.67}\text{Ca}_{0.33}\text{MnO}_3$  and  $\text{SrRuO}_3$ , have been prepared by the standard solid-state re-

action technique. A focused KrF excimer laser has been used for ablation, with a pulse energy of  $\sim 50$  mJ and a fluence of  $2-3$  J/cm<sup>2</sup> at the target. The films were deposited at a substrate temperature of  $650^\circ\text{C}$  in 200 mTorr oxygen. The deposition rates from the LCMO and SRO targets were calibrated against the number of laser pulses. Following deposition, the films were cooled down to room temperature at a rate of  $15^\circ\text{C}/\text{min}$  in 700 Torr  $\text{O}_2$ . The total thickness of the films is in the range of 500–1000 Å. The superlattices were grown according to designed layer thicknesses of each component. We designate a particular sample using the symbol of  $n/m$ , where  $n$  and  $m$  represent the number of unit cells (1 u.c.  $\sim 3.9$  Å) of LCMO and SRO, respectively.

We have characterized the pure LCMO and SRO films using Rutherford backscattering spectroscopy. The cation stoichiometry of the films were within 5% of the nominal target compositions. Transmission-electron micrographs confirmed the epitaxial growth of the LCMO film. We have analyzed the superlattices in the direction normal to the film surface using x-ray diffraction. The x-ray scans around the first-order diffraction peak are shown in Fig. 1 for the pure LCMO and SRO films with pseudocubic structure, and four LCMO/SRO superlattices with different stacking periodicities. Also presented in Fig. 1 is a simulated pattern (dashed line) for one of the superlattices, generated by using a commercial x-ray analysis software.<sup>16</sup> The unstrained lattice constants have been determined to be 3.86 Å and 3.94 Å for LCMO and SRO, respectively. If the films are epitaxially oriented with the in-plane lattice constant the same as that of the  $\text{SrTiO}_3$  substrate (3.905 Å), then the coherency strain is expected to result in a tetragonal distortion in the perpendicular  $c$ -axis direction with a decrease in the lattice constant

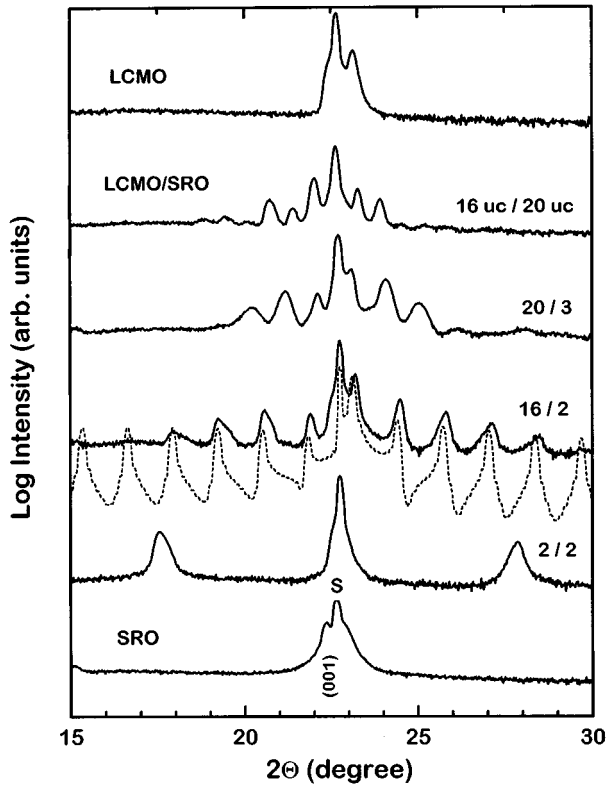


FIG. 1.  $\Theta$ - $2\Theta$  x-ray-diffraction patterns (log intensity scale) of the pure  $\text{La}_{0.67}\text{Ca}_{0.33}\text{MnO}_3$  and  $\text{SrRuO}_3$  films, and a series of superlattices with varying  $\text{SrRuO}_3$  layer thickness in units of unit cell (u.c.). The growth is along the  $c$  axis and the peak labeled "S" is from the  $\text{SrTiO}_3$  substrate. The dashed curve is a simulated pattern for the 16/2 superlattice assuming sharp interfaces.

for LCMO and an increase for SRO. The superlattices in Fig. 1 show the characteristic intense satellite peaks resulting from the modulation of multilayer structures. Even the film with layer thicknesses ( $t_{\text{LCMO}}$  and  $t_{\text{SRO}}$ ) of only two unit cells ( $\sim 7.8 \text{ \AA}$ ) shows an excellent satellite pattern. Qualitative agreement between the simulated and the measured peak positions and relative intensities has been obtained, suggesting that the actual stacking periodicities are close to the designed values. It should be noted that the simulated pattern is based on ideal superlattice structures with sharp interfaces. The discrepancies in the linewidths and relative intensities of the satellite peaks can result from some fluctuations in the layer thickness or cation interdiffusion across the interface.

The temperature ( $T$ ) dependence of the resistivity  $\rho(T)$  of some representative samples is shown in Fig. 2. For each sample,  $\rho(T)$  has been measured in zero field and in  $H=4 \text{ T}$ , with the field always parallel to both the film plane and the current direction. The LCMO film shows the familiar  $\rho(T)$  with a maximum MR ratio of about 400% (up to  $H=4 \text{ T}$ ) near  $T_c \approx 230 \text{ K}$ .<sup>10</sup> In sharp contrast, the SRO film in Fig. 1 shows a very small MR ratio ( $\sim 2\%$ ). Unlike LCMO, the  $\rho(T)$  of SRO does not display any dramatic transition across  $T_c$  of SRO which is about  $140 \text{ K}$ .<sup>13</sup> The slope change in  $\rho(T)$  near  $T_c$  is consistent with the conventional spin-disorder scattering in ferromagnetic metals. Comparing with LCMO, SRO is a much better conductor with substantially smaller  $\rho(T)$ . However, their residual  $\rho(0 \text{ K})$  are quite close to each other.

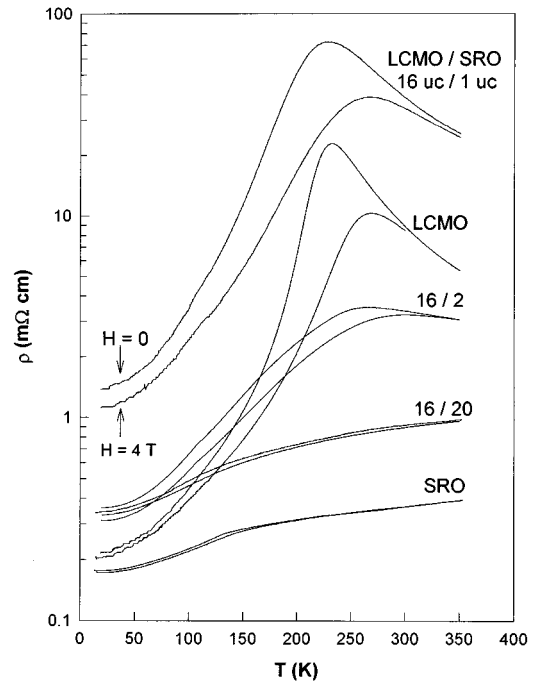


FIG. 2. Resistivity (in log scale) as a function of temperature for single layer films and superlattices. For each sample, data measured at both zero and 4 T fields are presented.

For the superlattice series in Fig. 2, we kept  $t_{\text{LCMO}}$  fixed at 16 u.c. while varying  $t_{\text{SRO}}$  from 1 to 20 u.c. The shape of  $\rho(T)$  for the 16/20 LCMO/SRO superlattice resembles that of the pure SRO film. This is because of the short-circuit effect of the better conducting SRO layers. As we reduce  $t_{\text{SRO}}$  in the superlattices, the shape of  $\rho(T)$  gradually approaches that of LCMO. However, the MR ratio in superlattices is enhanced at low  $T$  over the MR ratio of the pure LCMO. In fact, MR in the superlattices is much less sensitive to  $T$  unlike the MR in the LCMO film.

To clarify the evolution of the transport properties in the superlattices, we present in Fig. 3 two key parameters,  $\rho$  at 0 T and MR ratio ( $\Delta R/R_H$ ) at 4 T, as a function of  $t_{\text{SRO}}$ . With only 1 u.c. of SRO,  $\rho(300 \text{ K})$  initially increases threefold, but once  $t_{\text{SRO}}$  reaches 2 u.c. and above,  $\rho(300 \text{ K})$  drops abruptly. This indicates that continuous and conducting SRO layer starts to be formed at about 2 u.c., whereas, at the nominal  $t_{\text{SRO}}=1 \text{ u.c.}$ , SRO layers probably form discontinuous islands and behave as strong scatterers for the conduction electrons. Variation in  $t_{\text{SRO}}$  also affects the MR ratio dramatically. At  $T=225 \text{ K}$ , where pure LCMO possesses the maximum MR ratio, the value of  $\Delta R/R_H$  drops precipitously in the superlattices with increasing  $t_{\text{SRO}}$  as shown in Fig. 2. To understand this drop, we have modeled a superlattice as an assembly of classical parallel resistors. The dashed line in Fig. 2 is the simulated result of this model using the  $\rho$  and MR parameters of the pure LCMO and SRO films. The general trend is consistent with our experimental observation. However, there are deviations between the model prediction and the experimental data, presumably due to additional contributions to the parallel resistor model from interface scattering.

Perhaps the most interesting superlattice effect is the behavior of MR at low  $T$  (e.g., 20 K) as shown in Fig. 3. The

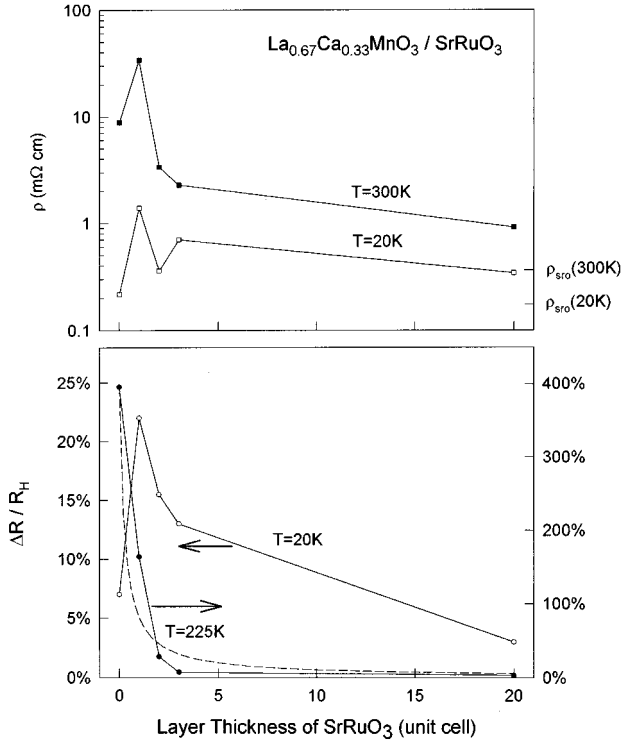


FIG. 3. Resistivity at 20 and 300 K, and magnetoresistance at 20 and 225 K, defined as  $[\rho_0 - \rho_{4T}]/\rho_{4T}$ , as a function of the layer thickness of SrRuO<sub>3</sub>. The layer thickness of La<sub>0.67</sub>Ca<sub>0.33</sub>MnO<sub>3</sub> is kept at about 16 unit cells. The dashed line is the simulated result of the MR ratio from the parallel resistor model.

superlattices with  $t_{\text{SRO}}=1, 2,$  and  $3$  u.c. all have enhanced  $\Delta R/R_H$  value over the pure LCMO film. In particular, the  $\Delta R/R_H$  value of the superlattice with  $t_{\text{SRO}}=1$  u.c. is enhanced by a factor of 3 to 22%. Since this enhancement only occurs at low  $T$ , it must be due to a different mechanism from the one which is responsible for the large MR near  $T_c$  ( $>200$  K). In other words, the low  $T$  magnetotransport relies more on a static magnetic structure as opposed to a dynamical one at high  $T$ . We believe that the low  $T$  enhancement in magnetotransport is due to the spin-dependent scatterings at the interfaces. As will be shown later, the spin structure in the superlattices is strongly influenced by the SRO layer. Consequently, a modulation of spin orientation may develop across the LCMO layer. For example, there may be a varying degree of spin canting at the interfaces of LCMO from the interior due to some degree of roughness or interdiffusion. The induced magnetic nonuniformity may cause the interfaces to provide additional spin-dependent scattering centers and enhance the MR ratio. It is desirable, in applications, to take advantage of interfaces or magnetic domain boundaries where magnetic nonuniformity is abundant. The strong magnetic scattering near these regions could substantially enhance the magnetotransport over a wide  $T$  range, hence reducing the thermal sensitivity of MR.

Because of the close relevance of magnetic structure to magnetotransport, it is important to study the magnetic properties of the LCMO/SRO superlattices. Both LCMO and SRO are FM metallic oxides with  $T_c=240$  and  $138$  K, respectively. However, the origin of ferromagnetism is different. The magnetic interaction is of the double-exchange type

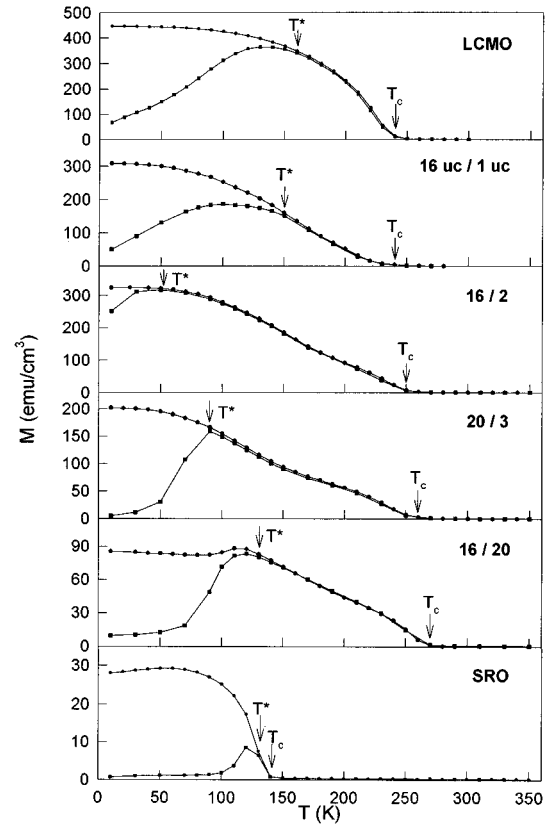


FIG. 4. Temperature dependence of the magnetization measured in a field of 150 G for a series of superlattices with increasing SrRuO<sub>3</sub> thickness. Both zero-field-cooled (warming-up) and field-cooled (cooling-down) curves are presented.

in LCMO, but not in SRO. Figure 4 shows the  $T$  dependence of magnetization ( $M$ ) measured at  $H=150$  G for the same series of superlattices presented earlier. For each sample, we have measured both the zero-field-cooled (ZFC) and the field-cooled (FC)  $M(T)$ . There are two interesting features in the  $M(T)$  data.

(1) The value of  $T_c$  of the LCMO layer ( $\sim 16$  u.c.) increases as  $t_{\text{SRO}}$  is increased. It ranges from 240 K in the sample with  $t_{\text{SRO}}=1$  u.c., to 270 K with  $t_{\text{SRO}}=20$  u.c. We note that the LCMO layers in the superlattices are under a biaxial tension due to a 2.1% lattice mismatch between LCMO and SRO. It is expected that the strain is more pronounced when the SRO layer is thicker. Our result is opposite to what has been observed in recent pressure studies of bulk LCMO and other manganites, in which it was found that  $T_c$  is increased by external hydrostatic pressure.<sup>17</sup> However, it should be noted that while in the superlattices the LCMO layers are biaxially expanded in the plane and compressed in the perpendicular direction, the hydrostatic pressure results in uniform reduction in volume.

(2) The thermal irreversible region between the zero-field-cooled (ZFC) and the field-cooled (FC)  $M(T)$  curves is sensitive to  $t_{\text{SRO}}$ . The characteristic temperature  $T^*$  as marked by arrows in Fig. 4, where irreversibility sets in, initially decreases as  $t_{\text{SRO}}$  is increased to 2 u.c., but afterwards it increases as  $t_{\text{SRO}}$  goes beyond 2 u.c. The thermal hysteresis seen here is possibly caused by some induced transitions in magnetic anisotropy.

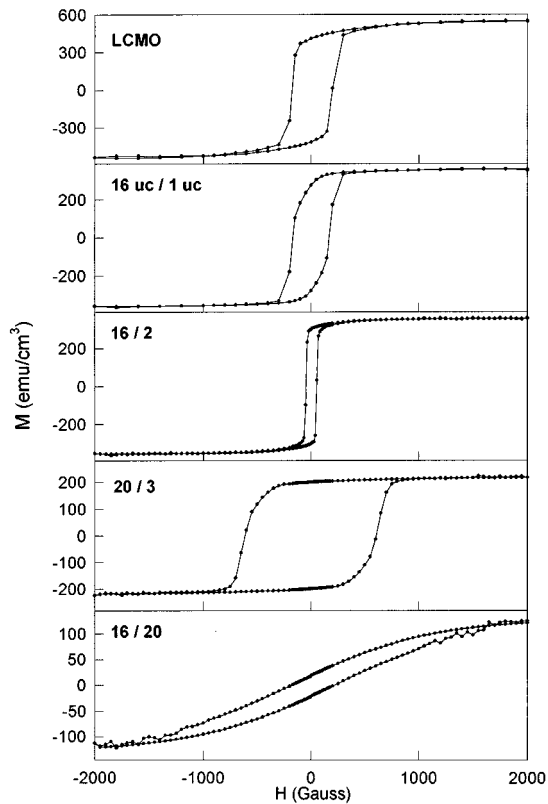


FIG. 5. Magnetic hysteresis loops measured at 5 K for the same series of superlattices shown in Fig. 4.

To elucidate the anisotropy, we have measured magnetic hysteresis loops at  $T=5$  K for the samples of interest, and the results are shown in Fig. 5 in the sequence of increasing  $t_{\text{SRO}}$ . During the measurements, the magnetic field is applied along the (100) direction in the plane of each epitaxial film. Starting from the pure LCMO film, the hysteresis loop is rounded and with a coercivity  $H_c=200$  G. We have confirmed that the easy axis is along (110) and the hysteresis loop along the (110) direction is close to a square. As  $t_{\text{SRO}}$  is increased from 0 to 2 u.c.,  $H_c$  decreases to 50 G and the hysteresis loop become squarelike. This means that the easy

axis has been switched to the (100) direction. Further increase in  $t_{\text{SRO}}$  by only one unit cell to 3 u.c. causes a dramatic increase in  $H_c$  to 600 G. The remanence of the superlattice with  $t_{\text{SRO}}=3$  u.c. is close to 95%, a clear indication of a (100) easy axis. Therefore, the magnetic characteristics of the LCMO/SRO superlattice ( $t_{\text{SRO}} \leq 3$  u.c.) seems to be determined by the competition between the (110) and (100) magnetic anisotropy. Finally, as we increase  $t_{\text{SRO}}$  to 20 u.c., it requires a much higher field to saturate  $M$  and the remanence is very small ( $\sim 15\%$ ). This is consistent with the fact that bulk (100)-SRO film has a perpendicular magnetic anisotropy,<sup>14</sup> possibly due to the inherent tetragonal distortion in the SRO film. So the magnetic anisotropy and its evolution in the LCMO/SRO superlattices is very rich in nature. Increasing  $t_{\text{SRO}}$  at unit cell level brings about two consecutive switchings of magnetic easy axis from (100) to (110), and to the  $c$  axis. In this sense, LCMO/SRO may serve as an excellent system to study magnetic interface anisotropy. The change in anisotropy is also the cause of the variation in the irreversible temperature  $T^*$  observed in Fig. 4. With the increase of  $t_{\text{SRO}}$ , the superlattices first become magnetically soft and then hard, which causes  $T^*$  to decrease initially and to increase later.

In summary, we have obtained high quality epitaxial  $\text{La}_{0.67}\text{Ca}_{0.33}\text{MnO}_3/\text{SrRuO}_3$  superlattices grown by pulsed laser deposition. An enhancement in the magnetoresistance ratio has been observed at low temperatures. We attribute this enhancement to the induced magnetic nonuniformity near the interfaces due to disorder, which serve as additional spin-dependent scattering centers. We have found that the tensile strain in the  $\text{La}_{0.67}\text{Ca}_{0.33}\text{MnO}_3$  layer drives up the magnetic phase transition temperature by as much as 30 K. Furthermore, the proximity of  $\text{SrRuO}_3$  layer brings about two consecutive switchings of magnetic easy axis in the superlattices, from (110) to (100), and finally along  $c$  axis as the  $\text{SrRuO}_3$  layer becomes thicker.

We wish to thank J. Z. Sun, Yu Lu, and W. J. Gallagher for discussions. This work was supported by National Science Foundation Grant Nos. DMR-9414160 and DMR-9258306 and IBM.

<sup>1</sup>G. H. Jonker and J. H. Van Santen, *Phys. Rev.* **16**, 337 (1950).  
<sup>2</sup>E. O. Wollan and W. C. Koehler, *Phys. Rev.* **100**, 545 (1955).  
<sup>3</sup>C. Zener, *Phys. Rev.* **82**, 403 (1951); P. W. Anderson and H. Hasegawa, *ibid.* **100**, 675 (1955); P. G. DeGennes, *ibid.* **118**, 141 (1960).  
<sup>4</sup>R. von Helmolt *et al.*, *Phys. Rev. Lett.* **71**, 2331 (1993).  
<sup>5</sup>K. Chahara *et al.*, *Science* **63**, 1990 (1993).  
<sup>6</sup>S. Jin *et al.*, *Appl. Phys. Lett.* **264**, 413 (1994).  
<sup>7</sup>R. Mahendiran *et al.*, *Solid State Commun.* **94**, 515 (1995).  
<sup>8</sup>G. Gong *et al.*, *Appl. Phys. Lett.* **67**, 291 (1995).  
<sup>9</sup>A. Gupta *et al.*, *Appl. Phys. Lett.* **67**, 3494 (1995).

<sup>10</sup>M. F. Hundley *et al.*, *Appl. Phys. Lett.* **67**, 860 (1995).

<sup>11</sup>J. M. Longo *et al.*, *J. Appl. Phys.* **39**, 1327 (1968).

<sup>12</sup>R. J. Bouchard and J. L. Gillson, *Mater. Res. Bull.* **7**, 873 (1972).

<sup>13</sup>C. B. Eom *et al.*, *Science* **258**, 1766 (1992).

<sup>14</sup>L. Klein *et al.*, *Appl. Phys. Lett.* **66**, 2427 (1995).

<sup>15</sup>M. Y. Chern *et al.*, *Appl. Phys. Lett.* **60**, 3045 (1992).

<sup>16</sup>Rocking Curve Analysis by Dynamic Simulation (RADS), Bede Scientific Instruments Ltd., Bowburn, Durham, UK.

<sup>17</sup>H. Y. Hwang *et al.*, *Phys. Rev. B* **52**, 15 046 (1995); K. Khazeni *et al.*, *Phys. Rev. Lett.* **76**, 295 (1996).